ESC European Society of Cardiology

European Heart Journal (2023) **44**, 304–318
https://doi.org/10.1093/eurheartj/ehac647

TRANSLATIONAL RESEARCH
Vascular biology and medicine

Vinculin phosphorylation impairs vascular endothelial junctions promoting atherosclerosis

Yu-Tsung Shih [1], Shu-Yi Wei[1†], Jin-Hua Chen[2†], Wei-Li Wang[1], Hsin-Yi Wu[3], Mei-Cun Wang[1], Chia-Yu Lin[1], Pei-Lin Lee[1], Chih-Yuan Lin[4], Hung-Che Chiang[5], Yu-Ju Chen[6], Shu Chien[7], and Jeng-Jiann Chiu [1,8,9]*

[1]Institute of Cellular and System Medicine, National Health Research Institutes, Miaoli 35053, Taiwan; [2]Graduate Institute of Data Science, College of Management, Health Data Analytics and Statistics Center, Office of Data Science, Biostatistics Center, Department of Medical Research, Wan Fang Hospital, Taipei Medical University, Taipei 11031, Taiwan; [3]Instrumentation Center, National Taiwan University, Taipei 10617, Taiwan; [4]Division of Cardiovascular Surgery, Tri-Service General Hospital, Taipei 114, Taiwan; [5]Department of Pharmacy, School of Pharmacy, China Medical University, Taichung 404327, Taiwan; [6]Academic Sinica, Institute of Chemistry, Taipei 11529, Taiwan; [7]Departments of Bioengineering and Medicine, and Institute of Engineering in Medicine, University of California, San Diego, La Jolla, CA 92093, USA; [8]School of Medical Laboratory Science and Biotechnology, Ph.D. Program in Medical Biotechnology, College of Medical Science and Technology, Taipei Heart Institute, Taipei Medical University, Taipei 11031, Taiwan; and [9]Institute of Biomedical Engineering, National Tsing Hua University, Hsinchu 30071, Taiwan

Received 8 November 2021; revised 26 August 2022; accepted 27 October 2022; online publish-ahead-of-print 16 November 2022

See the editorial comment for this article 'Vinculin phosphorylation modulates endothelial cell permeability: a new target for cardiovascular disease?', by F. Bonacina and G.D. Norata, https://doi.org/10.1093/eurheartj/ehac704.

Abstract

Background and aims Atherosclerosis preferentially develops in arterial branches and curvatures where vascular endothelium is exposed to disturbed flow. In this study, the effects of disturbed flow on the regulation of vascular endothelial phosphoproteins and their contribution to therapeutic application in atherogenesis were elucidated.

Methods Porcine models, large-scale phosphoproteomics, transgenic mice, and clinical specimens were used to discover novel site-specific phosphorylation alterations induced by disturbed flow in endothelial cells (ECs).

Results A large-scale phosphoproteomics analysis of native endothelium from disturbed (athero-susceptible) vs. pulsatile flow (athero-resistant) regions of porcine aortas led to the identification of a novel atherosclerosis-related phosphoprotein vinculin (VCL) with disturbed flow-induced phosphorylation at serine 721 (VCL^{S721P}). The induction of VCL^{S721P} was mediated by G-protein-coupled receptor kinase 2 $(GRK2)^{S29P}$ and resulted in an inactive form of VCL with a closed conformation, leading to the VE-cadherin/catenin complex disruption to enhance endothelial permeability and atherogenesis. The generation of novel apolipoprotein E-deficient ($ApoE^{-/-}$) mice overexpressing S721-non-phosphorylatable VCL mutant in ECs confirmed the critical role of VCL^{S721P} in promoting atherosclerosis. The administration of a GRK2 inhibitor to $ApoE^{-/-}$ mice suppressed plaque formation by inhibiting endothelial VCL^{S721P}. Studies on clinical specimens from patients with coronary artery disease (CAD) revealed that endothelial VCL^{S721P} is a critical clinicopathological biomarker for atherosclerosis progression and that serum VCL^{S721P} level is a promising biomarker for CAD diagnosis.

Conclusions The findings of this study indicate that endothelial VCL^{S721P} is a valuable hemodynamic-based target for clinical assessment and treatment of vascular disorders resulting from atherosclerosis.

* Corresponding author. Tel: +886 2 2736 1661 ext. 7600, Fax: +886 2 6638 7537, Emails: jjchiu@nhri.org.tw; jjchiu88@tmu.edu.tw
† Equal contribution.

Structured Graphical Abstract

Key Question

Atherosclerosis preferentially develops in arterial branches and curvatures where vascular endothelium is exposed to disturbed flow. However, the effects of disturbed flow on the signalling networks of phosphoproteins in endothelial cells (ECs) and their contribution to atherogenesis are still largely unknown.

Key Finding

Vinculin (VCL) was highly phosphorylated at S721 (VCL^{S721P}) by disturbed flow in cultured ECs and in the vascular endothelium of athero-susceptible regions in arteries. This disturbed flow-induced VCL^{S721P} was mediated by G-protein-coupled receptor kinase 2 to promote endothelial permeability and atherogenesis.

Take Home Message

Endothelial VCL^{S721P} and serum levels of VCL^{S721P} and VCL^{S721P}/VCL are promising molecular targets for clinical assessment and treatment of early atherosclerosis.

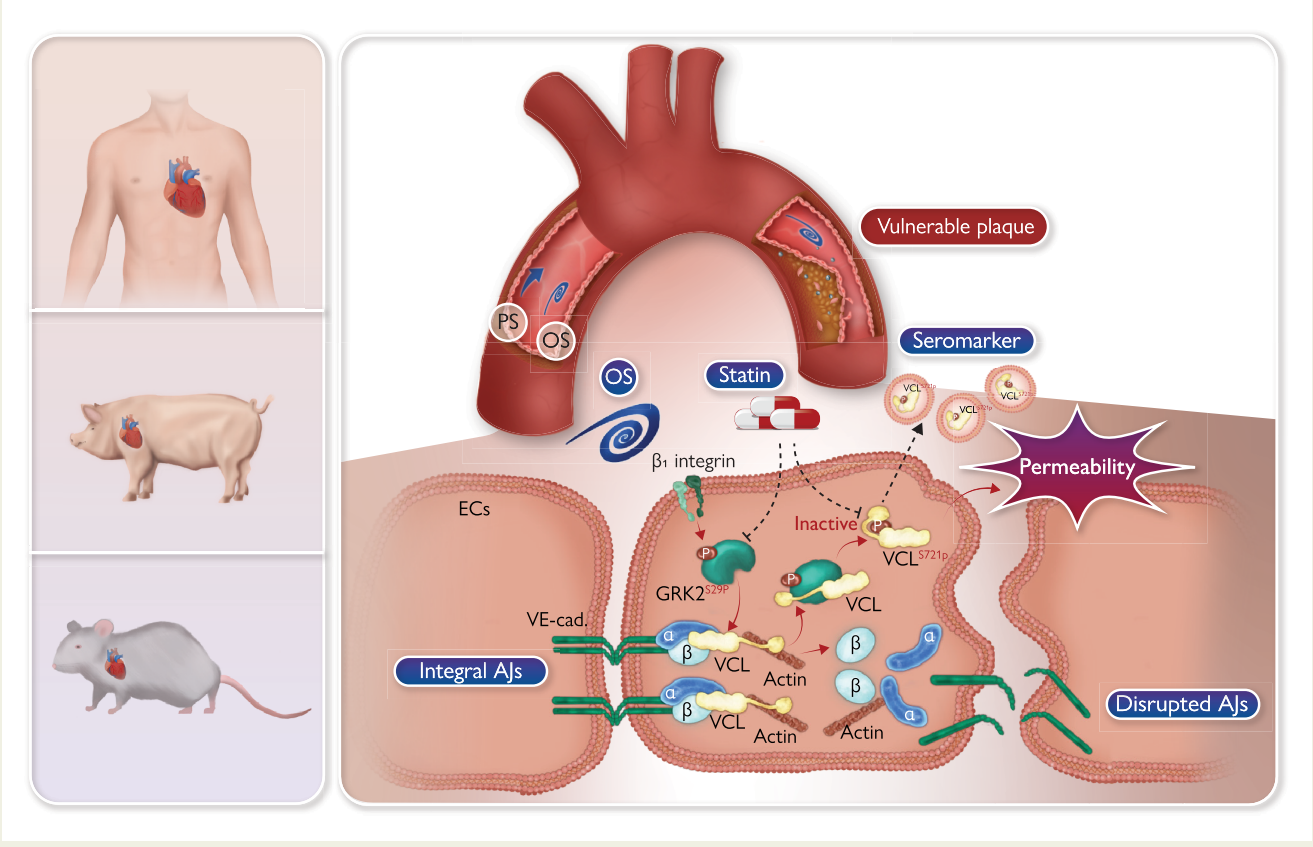

Proposed mechanisms by which disturbed flow induces vinculin phosphorylation at serine 721 (VCL^{S721P}) in vascular endothelium, leading to atherosclerosis. A combination of porcine models, large-scale phosphoproteomics, transgenic mice, and clinical specimens was used to demonstrate that disturbed flow induces endothelial VCL^{S721P} via G-protein-coupled receptor kinase 2 (GRK2)^{S29P}, resulting in an inactive form of VCL with a closed conformation. This disrupted the VE-cadherin junction/catenin complex to enhance endothelial permeability and atherosclerosis. Statin therapy was associated with reduced levels of sVCL^{S721P} and sVCL^{S721P}/sVCL in the serum of patients with coronary artery disease. Thus, endothelial VCL^{S721P} and serum levels of sVCL^{S721P} and sVCL^{S721P}/sVCL are promising molecular targets for the clinical assessment and treatment of atherosclerosis. AJ, adherens junction.

Keywords Atherosclerosis • Disturbed flow • Endothelial cell • Phosphoproteomics • Shear stress • Vinculin

Translational perspective

Atherosclerosis preferentially develops in arterial branches and curvatures where vascular endothelium is exposed to disturbed flow. In this study, we used porcine models, large-scale phosphoproteomics, transgenic mice, and human specimens to demonstrate that disturbed flow induces vinculin phosphorylation at S721 (VCL^{S721P}) in vascular endothelium to enhance endothelial permeability and atherosclerosis. VCL^{S721P} abundance was found to be positively correlated with atherosclerotic stages in clinical biopsies and sera from patients with coronary artery disease, suggesting that VCL^{S721P} abundance can be used as a seromarker to guide medication selection. Endothelial VCL^{S721P} is a promising target for clinical assessment and treatment of atherosclerosis.

Introduction

Cardiovascular disease (CVD) is a major cause of death and various disabilities worldwide, and atherosclerosis is a critical pathophysiological factor for CVD. Vascular endothelial dysfunction (ED), including increased vascular permeability and inflammation, initiates the early development of atherosclerotic lesions.[1] Since the clinical identification of ED is essential for preventing or reversing its progression to atherosclerotic disease, there is a need to develop new diagnostic biomarkers and therapeutic targets for clinical assessment and treatment of ED and atherosclerosis.

Force sensing by vascular endothelial cells (ECs) is critical for their biological functions. Clinical evidence revealed that areas of pulsatile flow with unidirectional shear stress (PS) in straight segments of the arterial tree are athero-resistant. In contrast, areas of disturbed flow with low and oscillatory shear stress (OS) at arterial branches and curvatures are prone to atherosclerosis.[2] However, the mechanism by which different flow patterns and shear stresses regulate molecular signaling and functions in ECs still needs to be elucidated. Protein phosphorylation, a necessary post-translational modification, is a critical regulatory mechanism associated with flow disturbances and atherogenesis.[3] Exposure of ECs to disturbed flow modulates the expression of various phosphoproteins, including $Smad1/5^{S463/S465P}$ (i.e. Smad1/5 phosphorylation at serine 463 and 465)[4] and $p65^{S536P}$, to induce endothelial proliferation and inflammation.[2] In contrast, pulsatile or laminar flow stimulates nitric oxide production by inducing endothelial nitric oxide synthase $(eNOS)^{S1177/S1179P}$;[5] this was associated with improved endothelial function in patients with coronary artery disease (CAD).[6] To discover new molecular targets and generate new approaches for the early diagnosis and treatment of atherosclerosis, it is necessary to determine the *in vivo* correlation between local phosphoprotein expression profiles in ECs and their athero-susceptibility in different flow areas.

Vinculin (VCL), a membrane-cytoskeletal protein involved in the linkage of integrins and the F-actin cytoskeleton, has been found to act as a mechanosensor that transmits forces to the cytoskeleton to maintain cell shape.[7] VCL controls cell motility by altering the cell's conformation from an inactive state, characterized by a tight head–tail interaction, to an active state in which intramolecular head–tail interaction is severed.[8] Deficiency of VCL reduces adhesion strength and results in defective cardiovascular development.[9] In contrast, VCL overexpression improves cardiac contractility and prolongs lifespan.[10] VCL can be phosphorylated at its tyrosine residues 100, 822, and 1065 in response to mechanical factors to induce its active form for contractile force transmission.[11] Investigations on plasma samples from patients with atherosclerotic disease showed up-regulation of VCL plasma levels in patients with acute coronary syndrome.[12] However, whether VCL phosphorylation can be differentially regulated by different flow patterns and shear stresses to contribute to atherogenesis remains unclear.

In this study, we used porcine models, large-scale phosphoproteomics, transgenic (Tg) mice, and human specimens to demonstrate that disturbed flow induces VCL phosphorylation at S721 (VCL^{S721P}) in vascular endothelium to promote atherosclerosis. Investigations on clinical biopsy specimens and sera from patients with CAD indicated that endothelial VCL^{S721P} is a critical clinicopathological biomarker for atherosclerosis progression and that the serum VCL^{S721P} ($sVCL^{S721P}$) level is a promising biomarker for CAD diagnosis. Our findings suggest that VCL^{S721P} may serve as a valuable hemodynamic-based target for clinical assessment and treatment of vascular disorders resulting from atherosclerosis.

Methods

Detailed materials and methods are provided in the online supplemental document. The experimental workflow is summarized in Supplementary material online, *Figure S1*.

Results

VCL^{S721P} is a novel atherogenic phosphoprotein in ECs that can be induced by disturbed flow *in vivo* and *in vitro*

Porcine vascular endothelia were harvested from the inner curvature (IA) (athero-susceptible, disturbed flow region) vs. the outer curvature (OA) of the aortic arch and the cranial part of descending thoracic aorta (TA) (athero-resistant, pulsatile flow regions) (see Supplementary material online, *Figure S2A*). EC purity was identified to be > 96% (see Supplementary material online, *Figure S2B* and *C*). These endothelia were subjected to quantitative large-scale phosphoproteomics analysis. A total of >1000 serine/threonine-phosphorylated peptides derived from >30 proteins were identified. We next identified atherosclerosis-related phosphoproteins that had (1) significant differences in expression between disturbed flow (i.e. IA) and pulsatile flow (i.e. OA and TA) regions and (2) no significant difference between the OA and TA regions. Threshold criteria of a >2-fold change ($\log_2$ fold change > 1) or <0.5-fold change ($\log_2$ fold change < −1) with a 99% confidence were used for the selection (see Supplementary material online, *Table S1*). Among these three regions, ECs from the IA expressed the highest levels of VCL^{S721P} and the lowest $eNOS^{S1179P}$ and $eNOS^{T1177P}$, compared with OA and TA (*Figure 1A*). Thus, VCL^{S721P} may be a critical pro-atherogenic phosphoprotein in ECs inducible by the disturbed flow.

To confirm the phosphoproteomics results on VCL^{S721P}, a VCL^{S721P}-specific rabbit polyclonal antibody was newly generated. Porcine ECs scraped from the IA exhibited higher levels of VCL^{S721P}

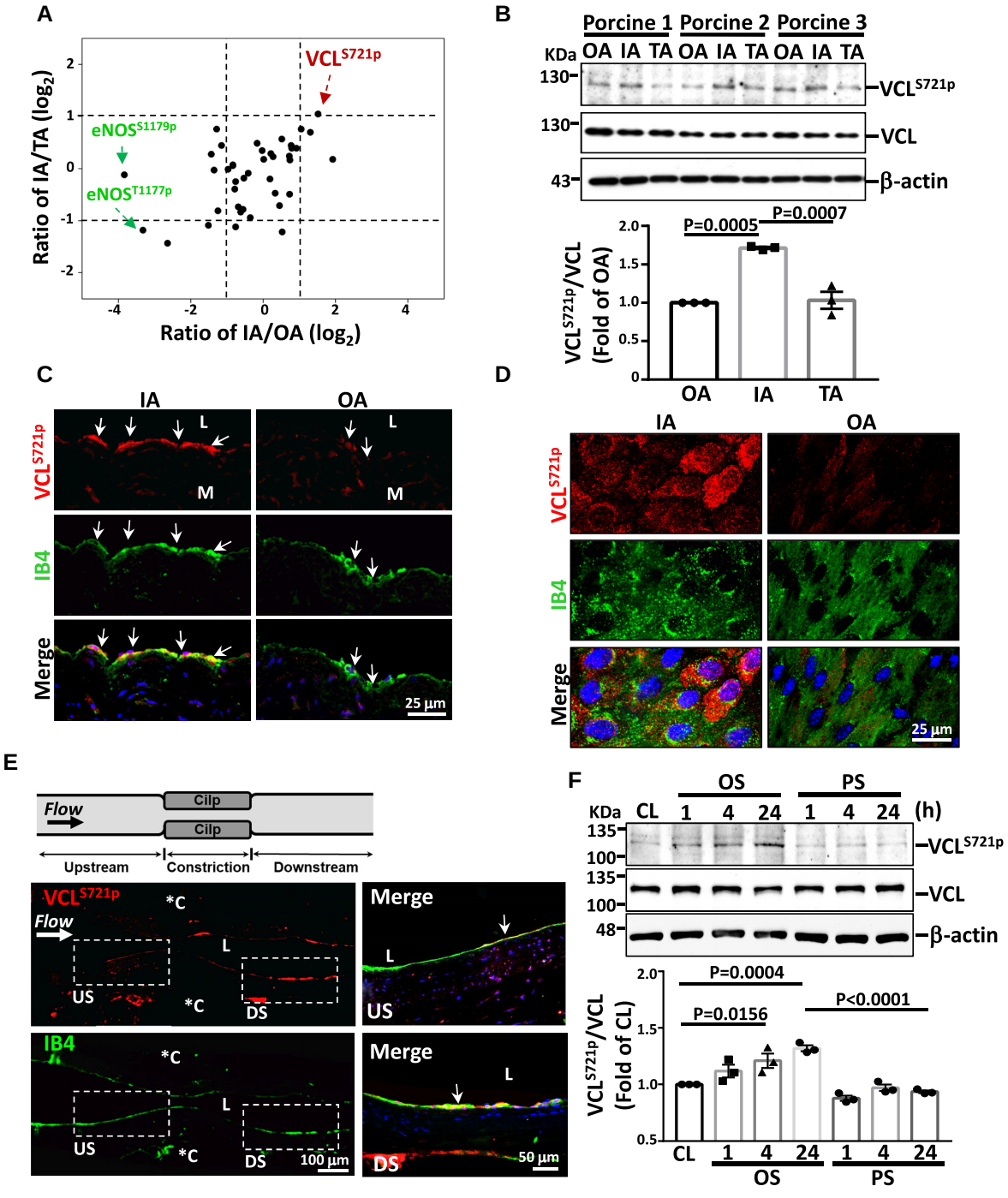

Figure 1 VCL^{S721p} is highly expressed in ECs exposed to disturbed flow *in vivo* and *in vitro*. (*A*) Approximately 10^7 cells were freshly scraped from the precisely defined areas of IA, OA, and TA of six pigs and subjected to large-scale phosphoproteomics analysis ($n = 3$). Results show the relative ratios of critical phosphoproteins in the IA compared with OA and TA. (*B–D*) Western blot analysis of VCL^{S721p} expression in fresh porcine aortic ECs (*B*, $n = 3$), immunohistochemical staining of the cross-sections of the porcine aortic arch (*C*), and *en-face* immunostaining of the *ApoE*$^{-/-}$ mouse aortic arch (*D*). (*E*) Longitudinally panoramic examination of EC VCL^{S721p} expression from the upstream (US) through the midpoint to the downstream (DS) areas of the constriction in the experimentally stenosed rat abdominal aorta. *C indicates clip-injured areas. Right panels show the magnified views of the indicated areas (white dashed line box). (*F*) ECs were kept under static condition as controls (CL) or subjected to oscillatory (OS) or pulsatile (PS) shear stress for the indicated times ($n = 3$). Arrows in *C* and *E* indicate the EC layer stained with an antibody against isolectin B4 (IB4). Data in *B* and *F* are means ± SEM and were analyzed by one-way ANOVA with Tukey multiple comparison test. The pictured images represent three independent experiments with similar results.

than those from the OA (*Figure 1B*); this finding was confirmed by immunohistochemical or *en-face* staining of porcine (*Figure 1C* and Supplementary material online, *Figure S3A*) and mouse (*Figure 1D* and Supplementary material online, *Figure S3B*) aortas. The *in vivo* induction of EC VCL^{S721P} by disturbed flow was further substantiated by immunohistochemical staining on the experimentally stenosed rat abdominal aorta (*Figure 1E*). These results showed that VCL^{S721P} was highly expressed in the EC layer at post-stenotic sites, where disturbed flow occurs.[4] *In vitro* flow chamber studies also showed that OS, but not PS, induced sustained expression of VCL^{S721P} in ECs (*Figure 1F*).

G-protein-coupled receptor kinase 2 (GRK2)^{S29P} is an active kinase responsible for disturbed flow induction of VCL^{S721P}

Motif-based analysis using Phospho Motif Finder and NetworKIN suggested that GRK2, a central signaling node that modulates G-protein-coupled receptors,[13] may be a potential upstream kinase for VCL^{S721P}. GRK2^{S29P}, the active form of GRK2,[14] was found to be highly expressed in vascular endothelium in porcine IA, but not OA or TA (*Figure 2A and B*, and Supplementary material online, *Figure S4*). This high induction of EC GRK2^{S29P} in the disturbed flow region was also observed in mouse IA (see Supplementary material online, *Figure S5A*) and post-stenotic sites of the stenosed rat abdominal aorta (*Figure 2C*); notably, it was co-localized with VCL^{S721P}. In flow channel studies, OS, but not PS, induced sustained expression of EC GRK2^{S29P} (*Figure 2D*) and its co-localization with VCL^{S721P} (see Supplementary material online, *Figure S5B*). This OS induction of GRK2^{S29P} was abolished by treating ECs with a GRK2-specific inhibitor (*Figure 2E* and Supplementary material online, *Figure S6A*) or transfecting with GRK2-specific siRNA (*Figure 2F* and Supplementary material online, *Figure S6B*); both of these processes also inhibited OS-induced VCL^{S721P}. GRK^{S29P} is an active upstream kinase of VCL^{S721P} in ECs that occurs in response to disturbed flow.

Disturbed flow induces an inactive form of VCL with a closed conformation

To investigate whether S721 phosphorylation of VCL affects its conformational changes, GFP-tagged wild-type VCL (VCL^{WT}), non-phosphorylatable mutant VCL^{S721A} (serine replaced by alanine), and phosphomimetic mutant VCL^{S721E} (serine replaced by glutamate) were constructed. We also generated full-length VCL FRET probes ($_{FRET}$VCL) in which ECFP (donor) was placed at the COOH terminus of the tail domain and EYFP (acceptor) was inserted into the end of the head domain (*Figure 3A*). Acceptor photobleaching of FRET probes in $_{FRET}$VCL^{WT}-transfected ECs exhibited low basal FRET levels. These results indicated that, under static conditions, VCL is in an active form with an open conformation (*Figure 3B and C*). Application of OS to $_{FRET}$VCL^{WT}-transfected ECs induced a conformational change of VCL from an active to inactive form, as indicated by the strong FRET signal in these ECs (*Figure 3B*). This OS-induced FRET signal was not observed in $_{FRET}$VCL^{S721A}-transfected ECs. Transfecting ECs with $_{FRET}$VCL^{S721E} probes also induced FRET signal in ECs, mimicking OS stimulation (*Figure 3B and C*). Blockage of VCL^{S721P} in ECs by treating with a GRK2 inhibitor diminished the OS-induced FRET signal (*Figure 3D and E*). Thus, our results indicate that disturbed flow and S721 phosphorylation induce an inactive form of VCL with a closed conformation, thus affecting endothelial permeability.

VCL^{S721P} induces endothelial permeability by disrupting VE-cadherin/catenin junctions

VCL prevents the opening of VE-cadherin/catenin junctions during their force-dependent remodeling.[15] High levels of VCL^{S721P} were correlated with disrupted VE-cadherin expression in ECs exposed to disturbed flow *in vitro* (*Figure 4A*) and in mouse IA *in vivo* (*Figure 4B*). Co-immunoprecipitation assays demonstrated that OS inhibited the association of VCL with VE-cadherin, α-catenin, and β-catenin in ECs (*Figure 4C*). These results were confirmed using the *in situ* proximity ligation assay (PLA). This process showed that OS inhibited direct associations of VCL with α-catenin and β-catenin in ECs (see Supplementary material online, *Figure S7*). Treating ECs with a GRK2-specific inhibitor inhibited the OS-induced increase in GRK^{S29P}/VCL^{S721P} association (*Figure 4D*) and decreases in VCL associations with VE-cadherin, α-catenin, and β-catenin (*Figure 4E*), while the VE-cadherin expression recovered from its disrupted pattern in the OS-stimulated cells (*Figure 4F*). An *in vitro* assay demonstrated that endothelial permeability was significantly increased by overexpression of phosphomimetic VCL^{S721E} in ECs (*Figure 4G*). This VCL^{S721P}-induced endothelial permeability was also confirmed using an *in vivo* endothelial permeability assay, which showed that administrating phosphomimetic VCL^{S721E} to *ApoE*$^{-/-}$ mice disrupted VE-cadherin expression and increased microsphere extravasation in mouse aortic ECs (see Supplementary material online, *Figure S8*). The disturbed flow-induced S721 phosphorylation of VCL in ECs impaired VE-cadherin/catenin junctions to increase EC permeability.

Inhibition of endothelial VCL^{S721P} reduces atherosclerotic lesions and increases their stability in $_{EC}$*Vcl*^{S721A}*ApoE*$^{-/-}$ mice

To investigate the *in vivo* pathophysiological roles of EC VCL^{S721P} in atherosclerosis, we generated novel $_{EC}$*Vcl*^{S721A} Tg *ApoE*$^{-/-}$ mice bearing EC-specific overexpression of non-phosphorylatable VCL^{S721A} in *ApoE*$^{-/-}$ background (see Supplementary material online, *Figure S9*). These Tg mice were equivalent in body mass, serum chemistry, and total plasma lipid profiles compared with inbred control *ApoE*$^{-/-}$ mice (see Supplementary material online, *Table S2*). Overexpression of EC VCL^{S721A} in $_{EC}$*Vcl*^{S721A}*ApoE*$^{-/-}$ mice significantly inhibited the opening of VE-cadherin junctions (*Figure 5A* and Supplementary material online, *Figure S10A*) and endothelial (*Figure 5B* and Supplementary material online, *Figure S10B*) and vascular permeabilities (see Supplementary material online, *Figure S10C*). These actions were accompanied by reduced atherosclerotic lesions (*Figure 5C*) and macrophage infiltration (*Figure 5D*). In comparison with control *ApoE*$^{-/-}$ mice, plaques from $_{EC}$*Vcl*^{S721A}*ApoE*$^{-/-}$ mice had reduced fibrous cap thickness (*Figure 5E* and Supplementary material online, *Figure S10D*), increased smooth muscle α-actin (αSMA)/Vimentin (Vim)-double-positive synthetic smooth muscle cells (SMCs) (*Figure 5F* and Supplementary material online, *Figure S10E*), and reduced necrotic core areas (*Figure 5G* and Supplementary material online, *Figure S10E*), whereas the collagen content was only slightly decreased (*Figure 5H* and Supplementary material online, *Figure S10F*). Moreover, the number of apoptotic cells in the plaque vascular endothelium in $_{EC}$*Vcl*^{S721A}*ApoE*$^{-/-}$ mice was significantly lower than that in control mice (*Figure 5I*). Taken together, our results indicate that knock-in of non-phosphorylatable VCL^{S721A} to decrease EC VCL^{S721P} expression

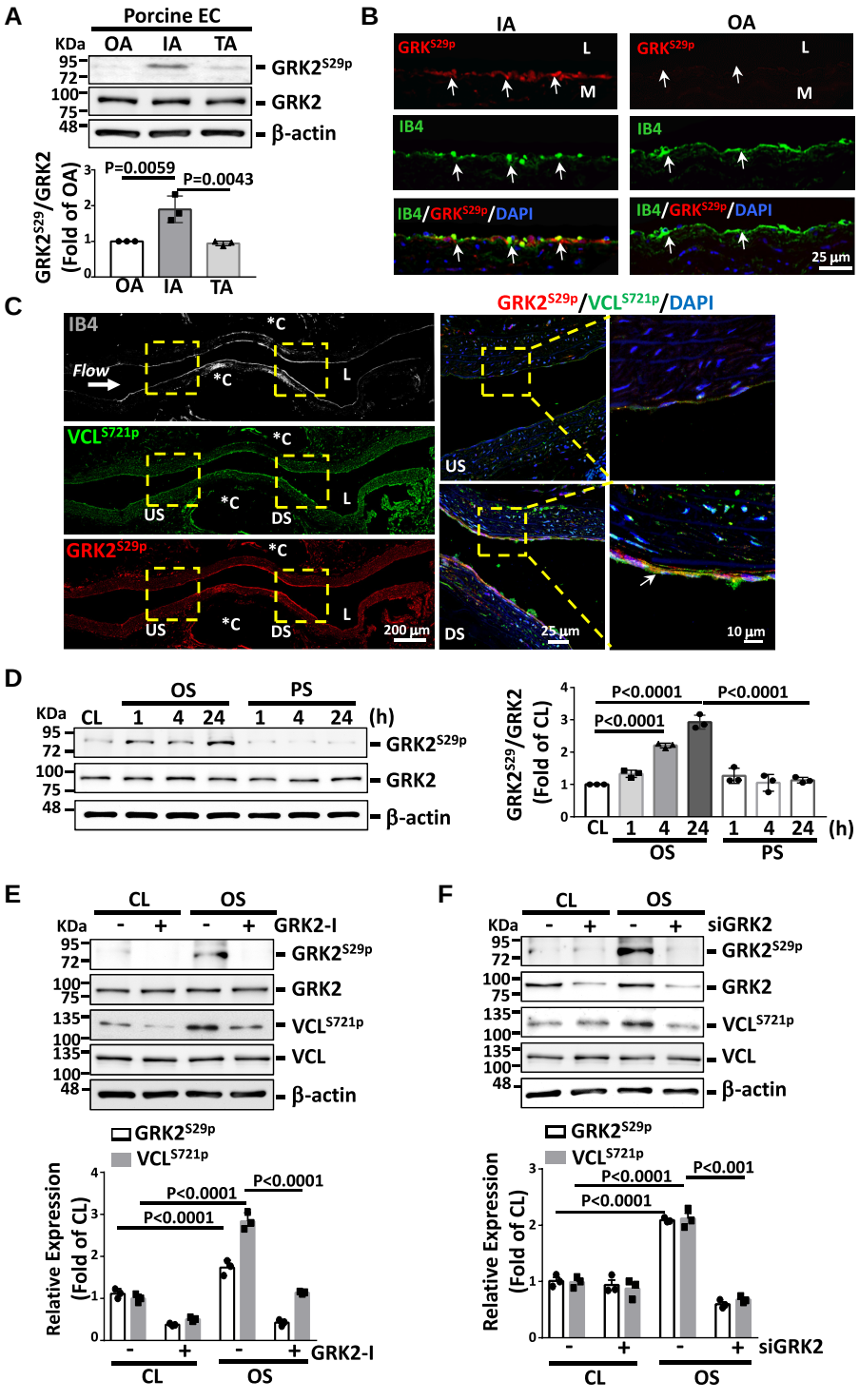

Figure 2 Disturbed flow induction of VCL^{S721p} is mediated by GRK2^{S29p}. (*A*) Western blot analysis of the expression of indicated proteins in fresh porcine aortic ECs. (*B*) Immunofluorescence staining for GRK2^{S29p} expression in the porcine IA and OA EC layers. Arrows indicate the EC layer stained for IB4. (*C*) Longitudinally panoramic examination of EC GRK2^{S29p} and VCL^{S721p} expressions from the upstream (US) through the midpoint to the downstream (DS) areas of the constriction in the experimentally stenosed rat abdominal aorta. Co-immunostaining for GRK2^{S29p} and VCL^{S721p} indicates their co-localization in ECs (arrows). *C indicates clip-injured areas. Right panels show the magnified views of the indicated areas (dashed line box). (*D–F*) ECs were kept under static condition as controls (CL) or subjected to oscillatory (OS) or pulsatile (PS) shear stress for the indicated times (*D*) or 24 h (*E* and *F*). In some experiments, ECs were pre-treated with GRK2-specific inhibitor (GRK2-I, 30 μM) (*E*) or transfected with GRK2-specific siRNA (siGRK2, 15 nM) (*F*) for 24 h. Data in *A*, *D–F* are means ± SEM ($n = 3$). One-way ANOVA with the Tukey multiple comparison test was applied to *A* and *D*. Two-way ANOVA with the Tukey multiple comparison test was applied to *E* and *F*. Results in each figure represent three independent experiments with similar results.

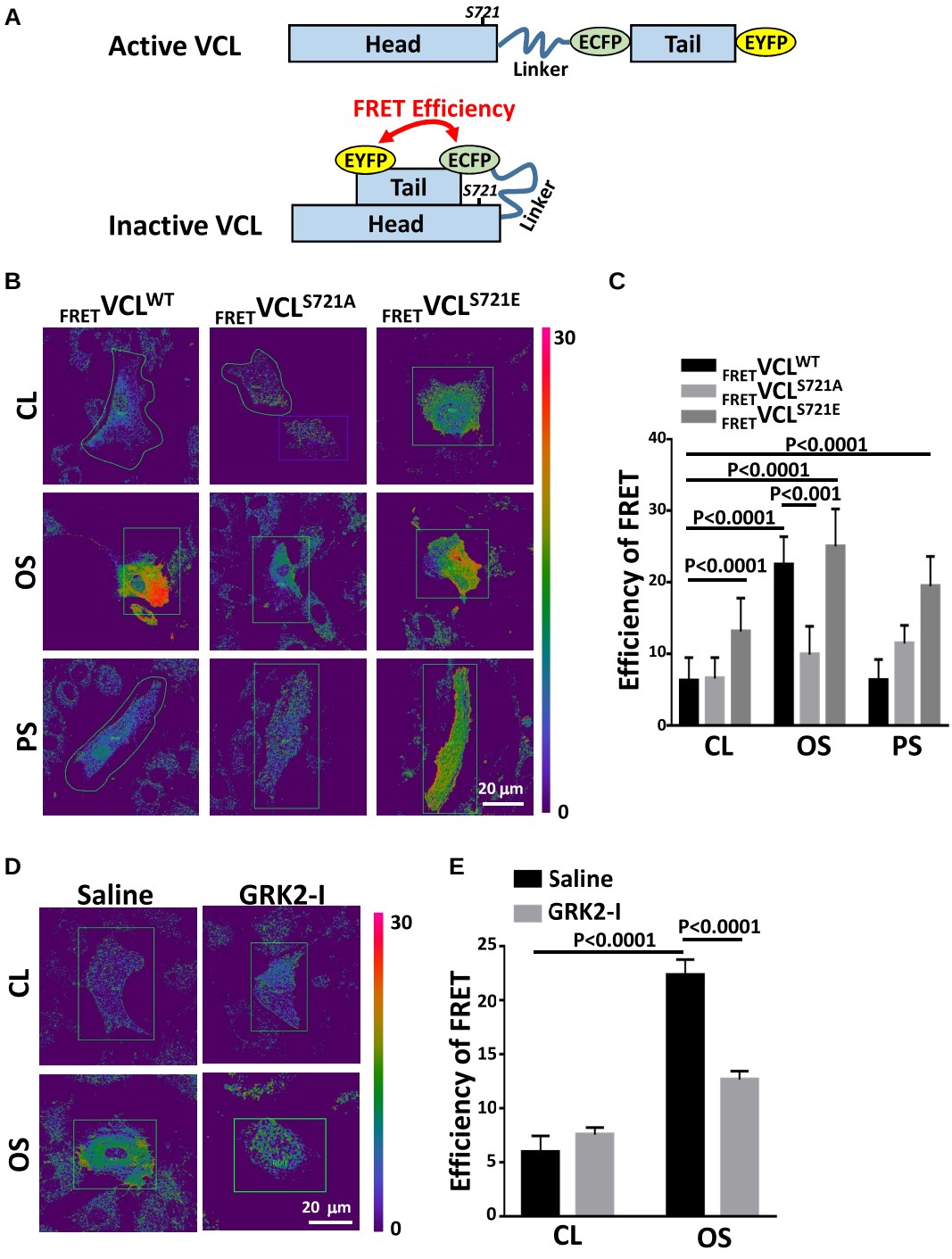

Figure 3 Disturbed flow induces an inactive form of VCL with a closed conformation. (*A*) Schematic diagrams showing the conformational changes of the VCL conformation-responsive FRET construct used in this study. Active VCL exhibits an open conformation in which intramolecular head–tail interaction is severed. Inactive VCL shows a closed conformation characterized by a tight head–tail interaction. Inactive VCL induces a high FRET signal, whereas the FRET signal is diminished for active VCL. (*B* and *C*) ECs were transfected with wild-type VCL FRET probe ($_{FRET}VCL^{WT}$) and mutant VCL FRET probes ($_{FRET}VCL^{S721A}$ and $_{FRET}VCL^{S721E}$) for 24 h and then kept under static condition as controls (CL) or subjected to oscillatory (OS) or pulsatile (PS) shear stress for 24 h. Pseudocolor FRET ratio images of these VCL FRET probes in live ECs were corrected after acceptor photobleaching (*B*), and the extracted FRET efficiencies were quantified ($n = 25$) (*C*). (*D* and *E*) $_{FRET}VCL^{WT}$-transfected ECs were incubated with GRK2 inhibitor (GRK2-I, 30 μM) or control saline for 24 h. These cells were kept under static condition as controls (CL) or subjected to oscillatory shear stress (OS) for 24 h, and their FRET pseudocolor signals were examined. The mean values of extracted FRET efficiency were quantified ($n = 15$) (*E*). Data in *C* and *E* are means ± SEM from three independent experiments and were analyzed by two-way ANOVA with Tukey multiple comparison test. The images in the figure represent three independent experiments with similar results.

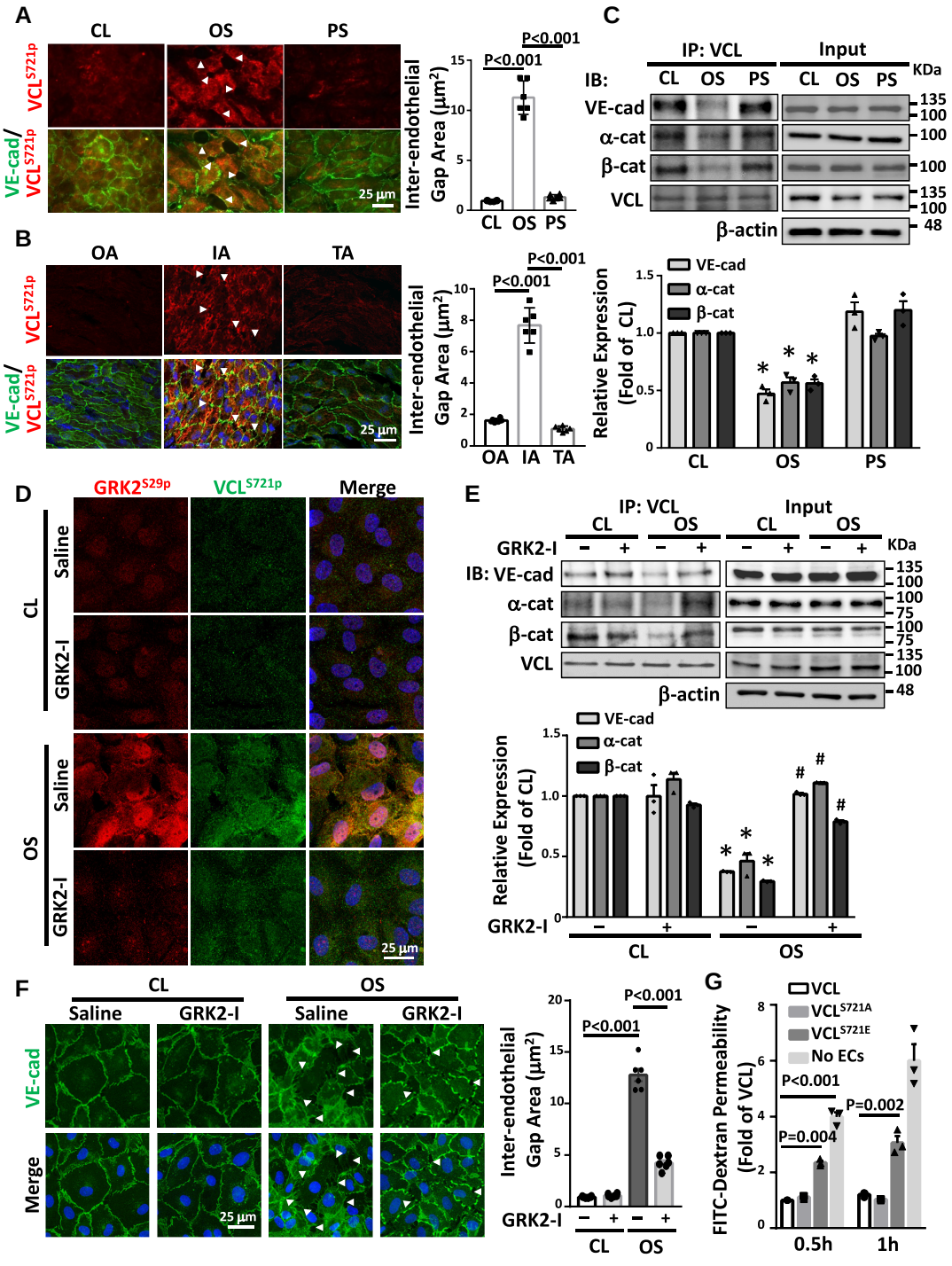

Figure 4 Disturbed flow induction of VCL^{S721p} increases EC permeability by disrupting VE-cadherin/catenin junctions. (*A*, *C–F*) Cultured ECs were kept under static condition as controls (CL) or subjected to oscillatory (OS) or pulsatile (PS) shear stress for 24 h. Cultured ECs (*A*) and EC monolayer in IA, OA, and TA of *ApoE*$^{-/-}$ mice (*B*) were *en-face* co-immunostained for VCL^{S721p} and VE-cadherin. (*C* and *E*) EC lysates were immunoprecipitated with VCL-specific antibodies, followed by Western blot analysis for VCL, VE-cadherin, α-catenin, β-catenin. *$P < 0.05$ vs. CL. $^{\#}P < 0.05$ vs. saline OS. (*D* and *F*) Representative results of GRK2^{S29p} and VCL^{S721p} co-immunostaining (*D*) and VE-cadherin immunostaining (*F*) in ECs. Cell nuclei were counter-stained with DAPI. In some experiments, ECs were pre-treated with a GRK2-specific inhibitor (GRK2-I, 30 μM) for 24 h (*D–F*). Arrowheads in *A*, *B*, and *F* indicate the gaps of inter-endothelial VE-cadherin junctions, and the gap areas were quantified. (*G*) Cultured ECs were transfected with VCL^{WT}, VCL^{S721E}, or VCL^{S721A}, and their permeability was assessed using the *in vitro* endothelial permeability assay with FITC-conjugated dextran (70 kDa). $n = 6$ for each group in *A*, *B*, and *F*, and $n = 3$ for other results. Data are means ± SEM from three to six independent experiments. One-way ANOVA with the Tukey test was applied to *A–C* and *G*. Two-way ANOVA with the Tukey multiple comparison test was applied to *E* and *F*. Results represent three to six independent experiments with similar results.

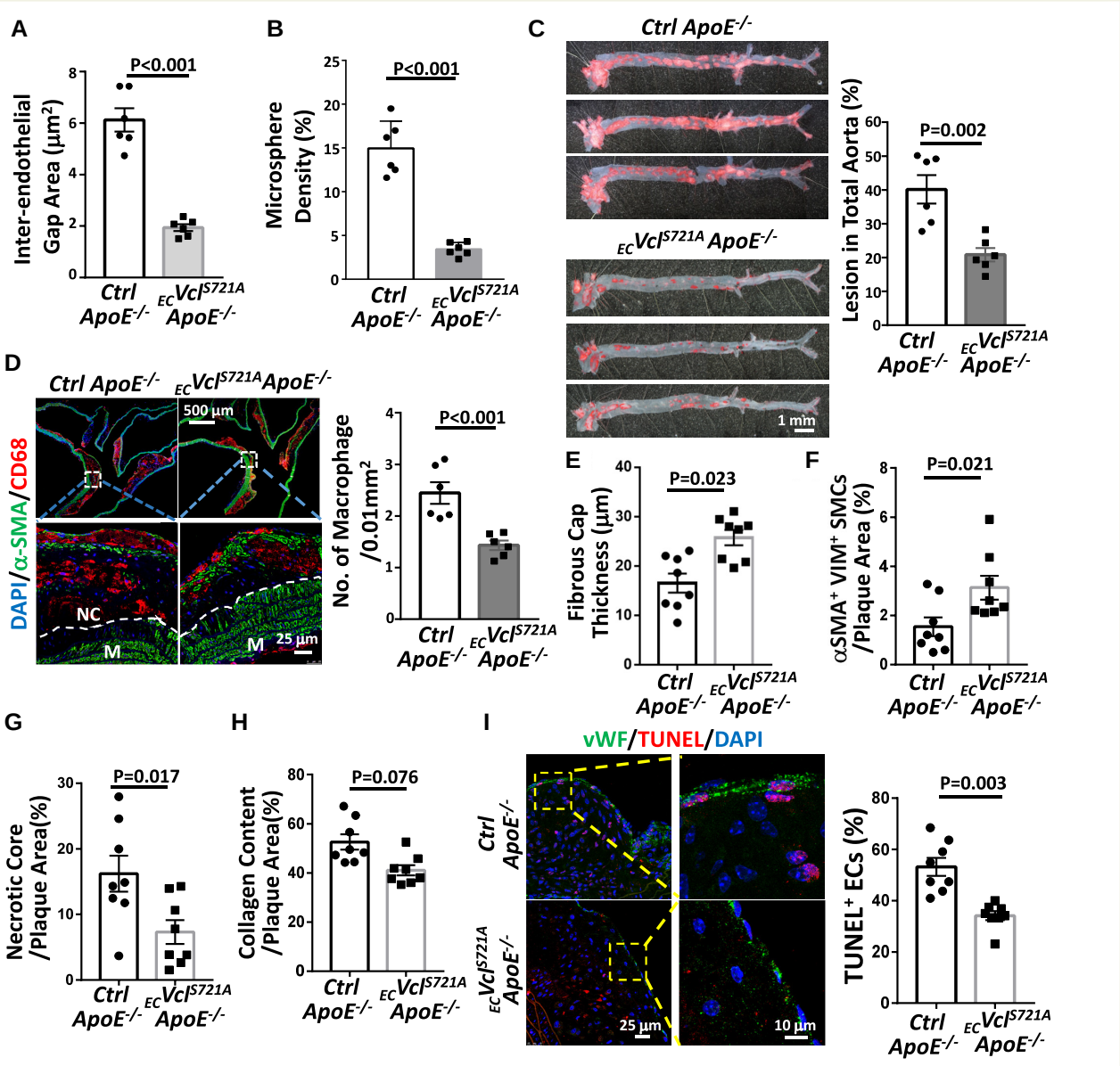

Figure 5 EC-specific overexpression of non-phosphorylatable mutant VCL^{S721A} in *ApoE*$^{-/-}$ mice reduces atherosclerotic lesions and increases plaque stability. $_{EC}$*Vcl*^{S721A}*ApoE*$^{-/-}$ and inbred control *ApoE*$^{-/-}$ mice were fed HCD for 6 weeks ($n = 6$ each), and their aortas were subjected to *en-face* co-immunostaining for DDK-tagged VCL^{S721A} and VE-cadherin. The inter-endothelial gaps between VE-cadherin junctions in the IA region were quantified (*A*). These mice were subjected to *in vivo* endothelial permeability assay using FITC-conjugated microspheres (G-spheres, 0.1 μm in size). The intensities of leaked microspheres in the endothelium of the IA region were quantified (*B*). (*C–I*) $_{EC}$*Vcl*^{S721A}*ApoE*$^{-/-}$ and inbred control *ApoE*$^{-/-}$ mice were fed HCD for 18 weeks ($n = 6$ each in *C* and *D*, $n = 8$ each in *E–I*). Whole segments of mouse aortas were subjected to Oil-red O staining to examine plaque formation (*C*). (*D*) Cross-sections of IA from these mice were co-immunostained for macrophage marker CD68 and SMC marker αSMA, with DAPI nuclear counterstains. Lower panels show magnified views of the indicated areas (dashed line box). The dashed lines indicate the margin of the tunica medial layer (*M*). NC, necrotic core. The number of infiltrated macrophages in the lesions was quantified ($n = 6$). (*E–I*) Quantifications of fibrous cap thickness by Movat pentachrome staining (*E*), synthetic SMCs within the lesions by co-immunostaining for αSMA and vimentin (VIM) (*F*), necrotic core areas (identified as the regions that lack DAPI-positive nuclei) by DAPI counterstaining (*G*), and collagen content by PicroSirus red staining (*H*). The representative images of *A*, *B*, *E*, *F*, *G*, and *H* are shown in Supplementary material online, *Figure S10A, B, D, E,* and *F*, respectively. (*J*) Apoptotic ECs identified by TUNEL staining, with vWF as an EC marker. The number of apoptotic ECs in plaques was quantified. The right panels in *I* are the magnified views of the indicated areas (dashed line box). All analyses in *E–I* were performed on the sections of the innominate artery and the IA region of mice. Data are shown as means ± SEM and were analyzed by a two-tailed Student *t*-test. Results represent six to eight independent experiments with similar results.

in *ApoE*$^{-/-}$ mice reduced atherosclerotic lesions and plaque vulnerability and increased plaque stability.

Administrating a GRK2 inhibitor to *ApoE*$^{-/-}$ mice reduces atherosclerotic lesions and increases plaque stability

The administration of a GRK2 inhibitor to *ApoE*$^{-/-}$ mice inhibited VCL^{S721P} expression and recovered VE-cadherin junction integrity in ECs (*Figure 6A* and Supplementary material online, *Figure S11A*), thereby inhibiting endothelial (*Figure 6B* and Supplementary material online, *Figure S11B*) and vascular (see Supplementary material online, *Figure S11C*) permeabilities. These responses were accompanied by reduced atherosclerotic lesions (*Figure 6C*) and macrophage infiltration (*Figure 6D*). GRK2 inhibitor administration also decreased collagen content (*Figure 6E* and Supplementary material online, *Figure S11D*), fibrous cap thickness (*Figure 6F* and Supplementary material online, *Figure S11E*), and necrotic core area (*Figure 6G* and Supplementary material online, *Figure S11F*), while increasing the number of αSMA^{+}Vim^{+} SMCs in plaques (*Figure 6H* and Supplementary material online, *Figure S11F*). GRK2 inhibitors also reduced the number of apoptotic cells in the plaque vascular endothelium (*Figure 6I*). There were no effects on body mass, serum chemistry, and plasma lipid profiles in *ApoE*$^{-/-}$ mice in response to GRK2 inhibitor administration (see Supplementary material online, *Table S3*). These results indicate that GRK2 inhibitors may have great potential as anti-atherosclerosis drugs.

Endothelial VCL^{S721P} serves as a clinicopathological marker for human atherosclerosis progression

To elucidate the clinical relevance of EC VCL^{S721P}, we examined the EC VCL^{S721P} levels and their correlation with the numbers of infiltrated macrophages in atherosclerotic lesions obtained from diseased human coronary arteries. According to American Heart Association guidelines for histological classification of atherosclerosis, diseased arteries contain six types of atherosclerotic lesions, ranging from mild lesions with fatty streaks to advanced lesions.[16] Serial sections of human atheromas were divided into three groups according to the following stages: initial neointima stage without macrophages (type I, group I), growing atheroma stage with intimal macrophages (types II–IV, group II), and advanced atheroma stage with fibrotic cap and calcification (types V–VI, group III) ($n = 15$–21 each). Compared with non-diseased arteries, VCL^{S721P} (*Figure 7A*) and GRK2^{S29P} (see Supplementary material online, *Figure S12A*) levels in the EC layers were increased in human atheromas, whereas the EC VE-cadherin expression was decreased. VCL^{S721P} and GRK2^{S29P} expressions were co-localized in ECs in groups II and III lesions (*Figure 7B*) and significantly higher than those in group I lesions (*Figure 7C*). Increased EC VCL^{S721P} (*Figure 7D*) and GRK2^{S29P} (see Supplementary material online, *Figure S12B*) were accompanied by the increased accumulation of invading macrophages in lesions. Interestingly, the numbers of CD68-positive macrophages were positively correlated with the level of EC VCL^{S721P} in all human lesion specimens examined (*Figure 7E*). VCL^{S721P} and GRK2^{S29P} levels in ECs were positively correlated with the numbers of macrophages infiltrated in human atherosclerotic lesions. These molecules may therefore serve as valuable clinicopathological markers for human atherosclerosis progression.

The levels of sVCL^{S721P} and its ratio to total sVCL in patients with CAD are promising biomarkers for CAD diagnosis

We further investigated the clinical relevance of VCL^{S721P} to human CVD by collecting sera from patients with CAD and healthy subjects (see Supplementary material online, *Figure S13*). One hundred and sixty-two individuals were divided into three groups (non-CAD, mild CAD, and moderate/severe CAD) following the CAD prognostic index[17] (see Supplementary material online, *Table S4*). All statistical data on clinical sera were analyzed using the multivariate linear regression model and adjusted for age, sex, smoking, body mass index, hypertension, diabetes, and hypercholesterolemia. In all cohorts, the levels of natural log-transformed (ln) sVCL^{S721P} (*Figure 8A*) and total sVCL (*Figure 8B*) from patients with CAD were significantly higher than those from non-CAD patients. Moreover, the sVCL^{S721P}/sVCL ratio in the moderate/severe CAD group was significantly higher than that in the non-CAD group (*Figure 8C*). We also analyzed sera from $_{EC}Vcl^{S721A}ApoE^{-/-}$ vs. inbred control *ApoE*$^{-/-}$ mice. The serum levels of sVCL^{S721P} and total sVCL in control *ApoE*$^{-/-}$ mice increased during atherosclerosis progression, while they decreased in $_{EC}Vcl^{S721A}ApoE^{-/-}$ mice compared with control *ApoE*$^{-/-}$ mice (see Supplementary material online, *Figure S14*). The vascular endothelium appeared to be the main contributor to the increased levels of sVCL^{S721P} and total sVCL during atherosclerosis progression.

The concentrations of sVCL^{S721P} and sVCL and the sVCL^{S721P}/sVCL ratio in the entire cohort were further analyzed based on the patients' medical records and medications. The results showed that patients taking statins had significantly lower levels of ln sVCL^{S721P} (*Figure 8A*) and sVCL^{S721P}/sVCL ratios (*Figure 8C*) than non-statin patients; treatments with β-blockers, calcium channel blockers, anti-platelet drugs, or fenofibrate showed no evidence of correlation with these biomarker levels, and they did not affect the ln sVCL level in patients with CAD (*Figure 8B*). These results suggest that sVCL^{S721P} and sVCL^{S721P}/sVCL levels are promising molecular targets for clinical assessment and treatment of atherosclerosis and that statin treatment is associated with the lower levels of sVCL^{S721P} and sVCL^{S721P}/sVCL in patients with CAD.

Discussion

Our *in vitro* and *in vivo* studies and investigations on human specimens have identified VCL^{S721P} as a novel mechanoresponsive phosphoprotein whose expression in ECs can be induced by disturbed flow to enhance EC permeability and atherogenesis. We selectively targeted VCL^{S721P} because: (1) VCL is an important mechanosensor whose phosphorylation plays a pivotal role in mechanotransduction and functional modulation in ECs. (2) Phosphoproteomics studies showed that ECs in athero-susceptible regions of aortas expressed higher levels of VCL^{S721P} than in athero-resistant regions. (3) VCL^{S721P} is highly expressed in the EC layer of human atherosclerotic coronary arteries, and its level is positively correlated with the number of macrophages that infiltrated atherosclerotic lesions. (4) The level of VCL^{S721P} and its ratio to total VCL in the serum of patients may be promising biomarkers for diagnosing CAD progression and medication selection. Thus, VCL^{S721P} is a valuable hemodynamic-based target for clinical assessment and treatment of atherosclerosis (*Structured Graphical Abstract*).

VCL is phosphorylated at Y100 and Y1065 to induce its active form with an open conformation.[11] However, the effects of different hemodynamic forces on VCL conformational changes and the specific residues that induce the inactive form of VCL have not been elucidated.

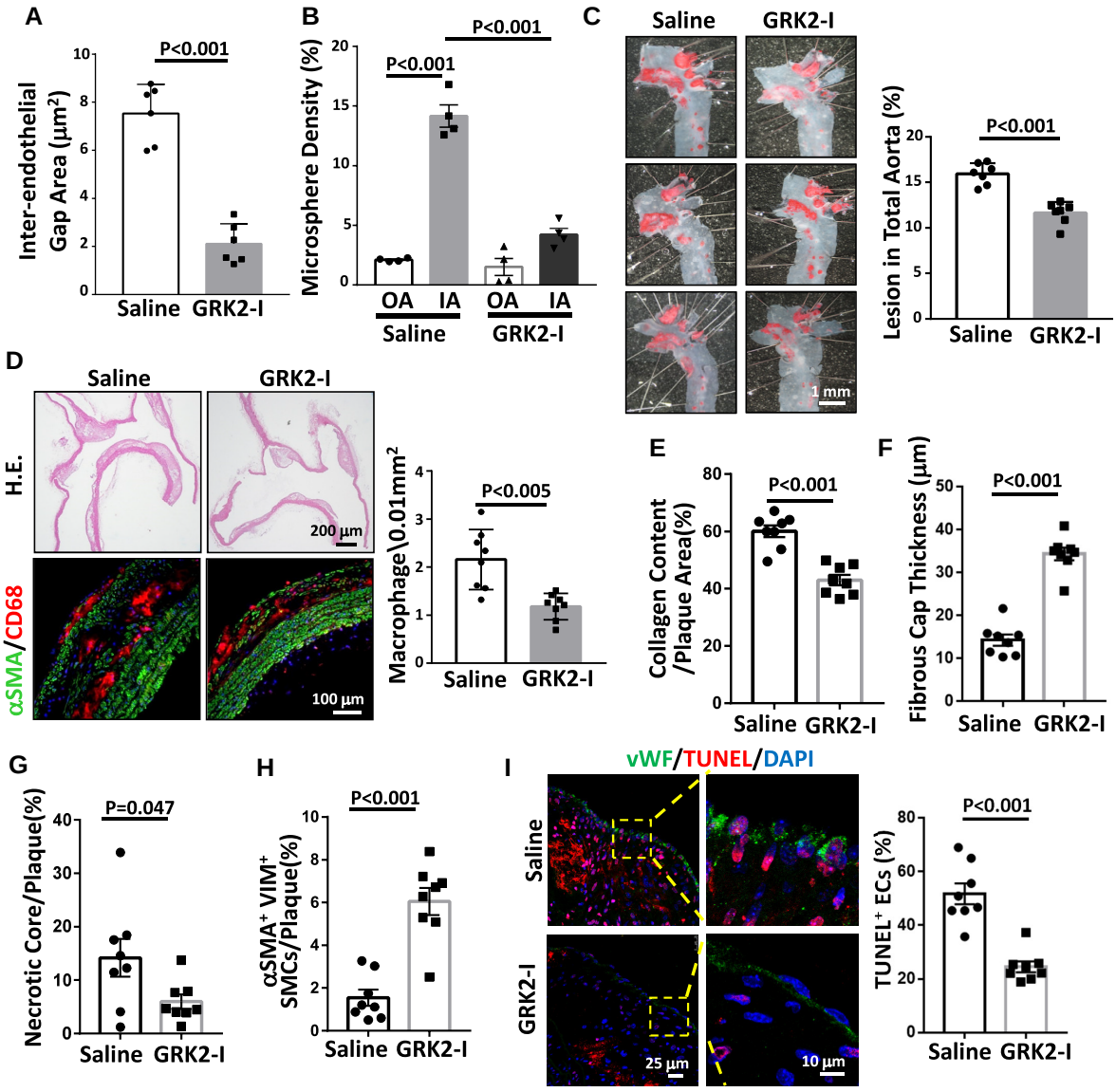

Figure 6 Administrating a GRK2-specific inhibitor to *ApoE*$^{-/-}$ mice reduces atherosclerotic lesions and increases plaque stability. *ApoE*$^{-/-}$ mice received vehicle control or GRK2-specific inhibitor (GRK2-I, 10 mg/kg IV every 3 d) for 6 (*A* and *B*), 12 (*C* and *D*), or 18 weeks (*E–I*). (*A*) Mouse aortas were subjected to *en-face* co-immunostaining for VCL^{S721P} and VE-cadherin with DAPI nuclear counterstains ($n = 6$). The inter-endothelial gaps between VE-cadherin junctions in the IA region were quantified. (*B*) Mice ($n = 4$) were subjected to *in vivo* endothelial permeability assay using FITC-conjugated microspheres. The intensities of leaked microspheres in the endothelium of the IA region were quantified. (*C*) Whole aortas were dissected and stained with Oil-red O to quantify lesion areas. (*D*) Serial longitudinal sections of aortas were stained with hematoxylin and eosin (upper panel). Macrophages infiltrated in lesions were determined by co-immunostaining for the macrophage marker CD68 and the SMC marker αSMA with DAPI nuclear counterstains (lower panel). The number of macrophages infiltrated in lesions was quantified ($n = 8$). (*E–I*) Quantifications of collagen content by PicroSirus red staining (*E*), fibrous cap thickness by Movat pentachrome staining (*F*), necrotic core areas (identified as the regions that lack DAPI-positive nuclei) by DAPI counterstaining (*G*), synthetic SMCs within the lesions by co-immunostaining for αSMA and vimentin (VIM) (*H*), and percentage of TUNEL-positive ECs on the lesions by co-immunostaining with TUNEL and vWF (*I*). The right panels in *I* are the magnified views of the indicated areas (dashed line box). The representative images of *A*, *B*, *E*, *F*, *G*, and *H* are shown in Supplementary material online, *Figure S11A, B, D, E,* and *F*, respectively. All analyses in *E–I* were performed on the sections of the innominate artery and the IA region of mice ($n = 8$ per group). Data are means ± SEM, and the images represent four to eight independent experiments with similar results. A two-tailed Student *t*-test was applied to *A* and *C–I*. One-way ANOVA with the Tukey multiple comparison test was applied to *B*.

The present results are the first evidence to suggest that VCL^{S721P} is an inactive form of VCL with a closed conformation in ECs in response to disturbed flow. This disturbed flow-induced conformational change of VCL disrupted the VE-cadherin/catenin complex to lead to increased EC permeability. These new findings provide novel mechanisms by which disturbed flow alters the phosphorylation status of VCL in ECs to impair junctional integrity, thus contributing to the pathogenesis of atherosclerosis.

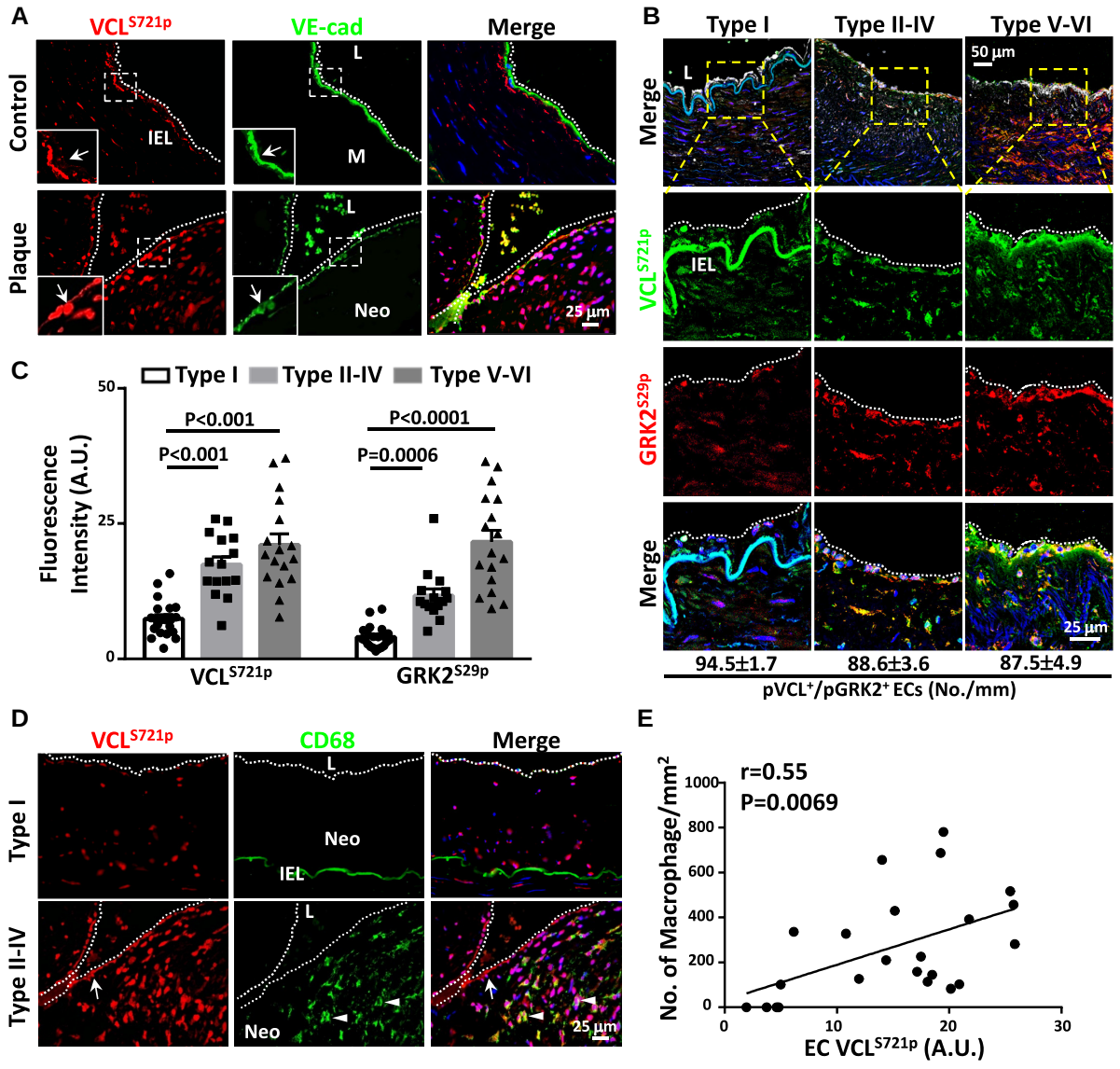

Figure 7 Atheroma plaques rich in CD68-positive macrophages exhibit higher EC VCL^{S721p} than initial lesions without intimal macrophages. (*A*) Cross-sections of diseased human coronary arteries and control internal thoracic arteries were co-immunostained for VCL^{S721p} and VE-cadherin. Left-lower panels in each picture show the magnified views of the indicated areas (white dashed line box). (*B*) Representative images of co-immunostaining for VCL^{S721p} and GRK2^{S29p}, followed by immunostaining for EC marker IB4 to examine VCL^{S721p}/GRK2^{S29p} co-localization in ECs. The lower panels in each group are the magnified views of the indicated areas (dashed line box) in the top panels. The numbers of ECs co-expressing VCL^{S721p} and GRK2^{S29p} were quantified ($n = 6$ in each group) and shown at the bottom. (*C*) Quantifications of average fluorescence intensity (arbitrary units, A.U.s) of EC VCL^{S721p} and GRK2^{S29p} in cross-sections of initial neointima lesions (type I, group I) ($n = 21$), growing atheromas (types II–IV, group II) ($n = 15$), and advanced atheromas (types V–VI, group III) ($n = 17$). (*D*) Cross-sections of different types of atheromas were co-immunostained for VCL^{S721p} and macrophage marker CD68. (*E*) Scatter plots showing a positive correlation between the average fluorescence intensities (arbitrary units, A.U.s) of EC VCL^{S721p} and the numbers of CD68-positive macrophages in the examined human atheroma sections ($n = 23$, $r = 0.5468$, $P = 0.0069$). *P*-values and correlation coefficients (r) were calculated by using the Spearman correlation test. Cell nuclei were counter-stained with DAPI. Data in *C* are means ± SEM and were analyzed by two-way ANOVA with Tukey multiple comparison test. Arrows in *A* and *D* indicate the VCL^{S721p}-positive EC layers. Arrowheads in *D* indicate CD68-positive macrophages. The dotted lines in *A*, *B*, and *D* indicate the margins of the vessel lumen. IEL, internal elastic lamina; L, lumen; M, medial region; Neo, neointima. Pictured images represent at least six independent experiments with similar results.

To the best of our knowledge, this is the first report to generate $_{EC}Vcl^{S721A}$ Tg *ApoE*$^{-/-}$ mice to investigate the *in vivo* pathophysiological roles of EC VCL^{S721p} in atherogenesis. Phenotypic studies indicated that these Tg mice were fully viable and without major anatomical defects and embryonic developmental effects. The areas of atherosclerotic lesions were significantly reduced in these Tg mice. In addition, the knock-in of non-phosphorylatable VCL^{S721A} to decrease VCL^{S721p} expression in ECs can inhibit EC apoptosis, reduce plaque vulnerability,

A

All Cohort (n=162)	Adjusted Estimate	ln(sVCL^{S721p}) ng/ml	95% CI	P Value
Mild (ref:Non)	0.89*		(0.39,1.39)	0.0006
Moderate/ Severe (ref:Non)	1.13*		(0.58,1.69)	<0.0001
Statin (ref: No)	-0.42*		(-0.8,-0.03)	0.0327
Antiplatelet (ref: No)	0.09		(-0.16,0.34)	0.4843
Beta Blocker (ref: No)	-0.22		(-0.49,0.06)	0.1194
CCB (ref: No)	0.29		(-0.14,0.71)	0.1855
Fibrate (Ref:No)	-0.68		(-1.51,0.15)	0.1063

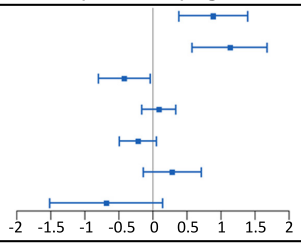

B

All Cohort (n=162)	Adjusted Estimate	ln(sVCL) ng/ml	95% CI	P Value
Mild (ref:Non)	0.55*		(0.13, 0.97)	0.0105
Moderate/ Severe (ref:Non)	0.53*		(0.07, 0.99)	0.025
Statin (ref: No)	0.05		(-0.27, 0.36)	0.7802
Antiplatelet (ref: No)	0.19		(-0.02, 0.4)	0.0753
Beta_Blocker (ref: No)	-0.07		(-0.3, 0.16)	0.5492
CCB (ref: No)	0.15		(-0.2, 0.51)	0.3992
Fibrate (Ref:No)	-0.07		(-0.76, 0.62)	0.8491

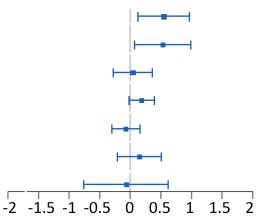

C

All Cohort (n=162)	Adjusted Estimate	sVCL^{S721p}/sVCLx100%	95% CI	P Value
Mild (red: Non)	12.76		(-6.42,31.93)	0.1906
Moderate/ Severe (ref: Non)	25.07*		(3.91,46.22)	0.0205
Statin (ref: No)	-22.66*		(-37.24,-8.08)	0.0025
Antiplatelet (ref: No)	-3.94		(-13.48,5.6)	0.4157
Beta Blocker (ref: No)	-10.05		(-20.47,0.38)	0.0588
CCB (ref: No)	3.81		(-12.44,20.06)	0.644
Fibrate (Ref:No)	-16.28		(-47.91,15.36)	0.3109

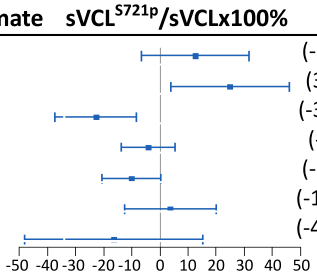

D

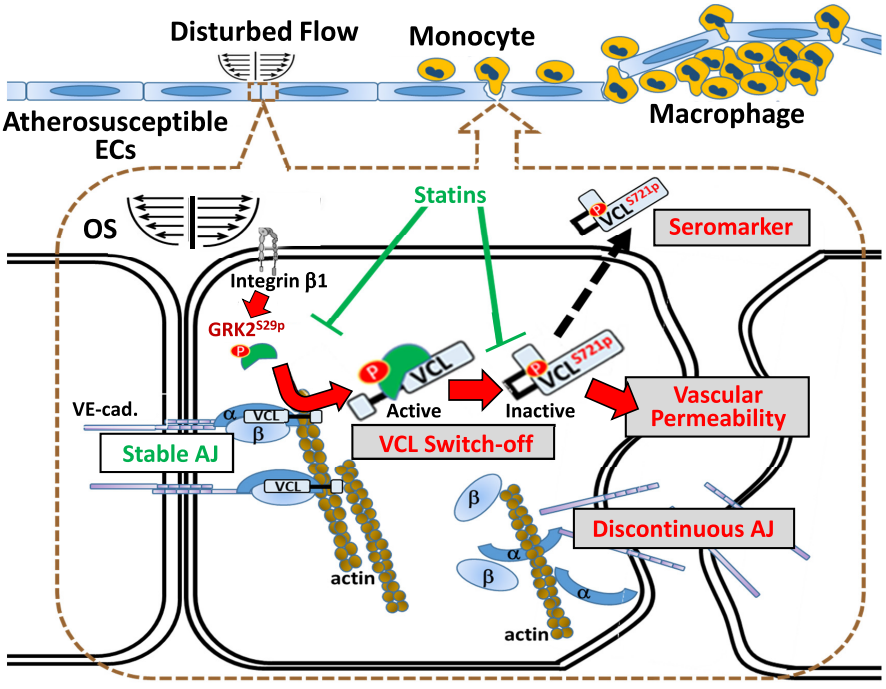

Figure 8 sVCL^{S721p} serves as a promising biomarker for CAD diagnosis. Measurements of the levels of sVCL^{S721p} and sVCL in the serum samples from the study cohort. Whole serum samples from the study cohort (see Supplementary material online, *Table S4*) were subjected to ELISA with antibodies against VCL^{S721p} and total VCL. All data were analyzed using the multivariate linear regression model and adjusted with multiple parameters, including age, sex, smoking, body mass index, hypertension, diabetes, and hypercholesterolemia. (*A–C*) The forest plots of the associations between different CAD severities or clinical drug therapies and the levels of sVCL^{S721p} (*A*), sVCL (*B*), or sVCL^{S721p}/sVCL (*C*) in all cohorts ($n = 162$). The distributions of sVCL^{S721p} (*A*) and sVCL (*B*) were skewed, and a natural log transformation (ln) was performed before statistical analysis. (*D*) Schematic diagram summarizing the mechanisms by which disturbed flow induces vinculin phosphorylation at S721 residue in vascular endothelium and contribute to atherosclerosis development.

and increase its stability. Thus, our findings suggest that inhibiting endothelial VCL^{S721p} may enhance vascular integrity, reduce the number of invading macrophages and markers of vulnerability, and increase atherosclerotic plaque stability.

Interestingly, GRK2^{S29p} appears to be an active upstream kinase that regulates VCL^{S721p} in ECs in response to disturbed flow. The pivotal role of GRK2 in modulating VCL^{S721p} was supported by GRK2 gain- and loss-of-function experiments that used its overexpression plasmid and specific siRNA, respectively (see Supplementary material online, *Figure S15*). GRK2 inhibition is a potential therapeutic strategy for CVD.[18] In the present study, the blockage of EC GRK2^{S29p} by its specific inhibitor inhibited the disturbed flow-induced EC VCL^{S721p} and atherosclerotic lesion formation and increased plaque stability. Our findings advance the notion that GRK2^{S29p} inhibition may treat vascular disorders resulting from atherosclerosis.

The GRK2 inhibitor may exert atheroprotective effects through a VCL-independent pathway. GRK2 administration can elevate the systemic levels of several inflammatory cytokines in the serum of *ApoE*$^{-/-}$ mice (see Supplementary material online, *Figure S16A*) and increase plaque areas (see Supplementary material online, *Figure S16B*). No significant difference in the expression profiles of circulating cytokines between $_{EC}$*Vcl*^{S721A}*ApoE*$^{-/-}$ and control *ApoE*$^{-/-}$ mice was observed (see Supplementary material online, *Figure S16C*). Moreover, proteins other than VCL, such as eNOS^{S1177p} and caveolin-2^{S23p}, which were differentially regulated in IA vs. OA (see Supplementary material online, *Table S1*), may also be affected by GRK2 activation (see Supplementary material online, *Figure S17*). Thus, administrating GRK2 to *ApoE*$^{-/-}$ mice may produce VCL-independent effects to induce vascular inflammation, thereby promoting atherosclerosis.

Studies by us[19] and others[20] have shown that $\alpha_5\beta_1$ and $\alpha_v\beta_3$ integrins are pivotal mechanoreceptors that transmit extracellular stimuli into intracellular signaling to regulate EC functions. Exposure of ECs to OS, but not PS, induced sustained activations of β_1 and β_3 integrins in ECs (see Supplementary material online, *Figure S18A*). Knockdown of β_1, but not β_3, integrin significantly inhibited OS-inductions of EC GRK2^{S29p} and VCL^{S721p} (see Supplementary material online, *Figure S18B and C*). These results suggest that β_1 integrin may be involved in OS-induced GRK2^{S29p}/VCL^{S721p} signaling cascade in ECs.

The phenotypic switch of SMCs to macrophage-like cells is an essential mechanism in atherosclerosis pathology.[21,22] In this study, αSMA$^+$CD68$^+$ cells represented only approximately 4–5% of all αSMA$^+$ cells in all animal models tested. In all human lesion specimens examined, there was no correlation between the number of αSMA$^+$CD68$^+$ cells in plaques (see Supplementary material online, *Figure S19A*) and EC VCL^{S721p} (see Supplementary material online, *Figure S19B*) or GRK2^{S29p} (see Supplementary material online, *Figure S19C*) levels. In contrast, there was a positive correlation between the number of αSMA$^+$CD68$^-$ cells in plaques and EC VCL^{S721p} (see Supplementary material online, *Figure S19D*) and GRK2^{S29p} (see Supplementary material online, *Figure S19E*) levels. These results suggest that the VCL^{S721p} and GRK2^{S29p} levels in ECs may not be associated with SMC phenotypic switch to macrophage-like cells in atherosclerotic plaques.

This is the first study to show that VCL^{S721p} is highly expressed in the endothelium of human atheroma and that its level and ratio to total VCL in the serum of patients with CAD are increased during atherosclerosis progression. The mechanisms by which VCL^{S721p} and VCL are released into plasma remain unclear. sVCL may be contained in exosomes or extracellular vesicles (EVs) released from prostate cancer cells.[23] In addition, VCL could be proteolyzed into a cleaved fragment (~95 kDa) by a specific protease calpain.[24] Most sVCL^{S721p} and sVCL present in serum were in the full-length form (~124 kDa), and only a minority were in the cleaved form (~95 kDa) (*Figure 14A*). Both full-length and cleaved forms of sVCL^{S721p} and sVCL were detected in EVs and CD9$^+$ exosomes in the $_{EC}$*Vcl*^{S721A}*ApoE*$^{-/-}$ and control *ApoE*$^{-/-}$ mice serum (see Supplementary material online, *Figure S20A*). Moreover, *en-face* immunostaining showed that μ-calpain (i.e. the active form of calpain) was highly expressed in the vascular endothelium of the IA in comparison with OA (see Supplementary material online, *Figure S20B*). Disturbed flow may induce the expression of active calpain in ECs. Our findings provide new insights into the changes in the expression of essential molecules in the arterial endothelium during atherosclerosis progression, which can eventually be transformed into measurable fingerprints in plasma.

Interestingly, we found that statin therapy was associated with reduced levels of ln sVCL^{S721p} and sVCL^{S721p}/sVCL in the entire study cohort. Statin exerts pleiotropic effects to inhibit EC dysfunction and atherosclerosis.[25] Atorvastatin treatment inhibited OS-induced GRK2^{S29p} and VCL^{S721p} in cultured ECs (see Supplementary material online, *Figure S21A–C*). The administration of atorvastatin to *ApoE*$^{-/-}$ mice inhibited endothelial inductions of GRK2^{S29p} and VCL^{S721p} and atherosclerosis development (see Supplementary material online, *Figure S21D–F*). These results suggest that statins may exert atheroprotective effects, at least in part, via the inhibition of disturbed flow-induced EC GRK2^{S29p}/VCL^{S721p} signaling cascade. Compared with statin therapy alone, we found no evidence of synergistic or additive effects of combined therapy of statins with other drugs on reductions of ln sVCL^{S721p} and sVCL^{S721p}/sVCL levels. Further investigations are needed to determine which specific drug combinations have synergistic or additive effects.

There were several limitations to our study. First, the Tie-2 promoter used in $_{EC}$*Vcl*^{S721A}*ApoE*$^{-/-}$ mice might not be specific to ECs.[26] The use of the Tie-2 promoter did not affect VCL^{S721p} and VCL expressions in other tissues (see Supplementary material online, *Figure S9E*). However, its effect on different cell types such as macrophages cannot be excluded. Second, VCL phosphorylation is complex, with multiple functional and structural states. Previous studies reported that VCL^{Y100p}, VCL^{Y1065p}, and VCL^{Y822p} regulated focal adhesions, actin filament assembly, and cell spreading.[11] In human pathophysiology, these post-translational modifications may regulate vinculin function in an integrated manner. Third, in humans, the coronary or carotid arteries are typically responsible for clinical events and the focus of stenting treatments.[27] Phosphoproteomics studies using coronary or carotid arteries are needed to match our findings with current clinical practices. Fourth, this study was limited by the small number of human samples; hence, further studies with many patients are warranted.

In summary, VCL was highly phosphorylated at its S721 residue in ECs by disturbed flow, consequently promoting EC permeability and atherosclerosis (summarized in *Figure 8D*). EC VCL^{S721p} may serve as a promising hemodynamic-based target for clinical assessment and treatment of vascular disorders resulting from atherosclerosis.

Author contributions

Y.-T.S., S.-Y.W., W.-L.W., M.-C.W., C.-Y.L., and P.-L.L. carried out experimental work. Y.-T.S. analyzed data. H.-Y.W. and Y.-J.C. performed phosphoproteomics. Y.-T.S. and J.-J.C. designed experiments. C.-Y.L. and H.-C.C. provided human specimens and participated in the

discussion. J.-H.C. helped with the statistical analysis of clinical data. Y.-T.S., S.C., and J.-J.C. participated in the discussion and wrote the manuscript.

Supplementary material

Supplementary material is available at *European Heart Journal* online.

Acknowledgements

We thank Taiwan Pigmodel Animal Technology Co., Ltd. for providing experimental porcine samples. We also thank the National Laboratory Animal Center and the NHRI Core Facilities for transgenic animal generation and technical support. We thank Ms Yi-Ju Ko, Chih-I Lee, Pei-Fen Chen, and Ching-Wen Tsai for their technical support, human serum samples, and statistical data analysis.

Funding

This work was supported by the Taiwan Ministry of Science and Technology grants MOST 109-2326-B-400-006 and 109-2320-B-400-010-MY3 (to J.-J.C.) and the National Institutes of Health grant R01HL108735 (to S.C.).

Conflict of interest: The authors declare that there is no conflict of interest.

Data availability

The article's data will be shared upon reasonable request to the corresponding author.

References

1. Corban MT, Lerman LO, Lerman A. Ubiquitous yet unseen: microvascular endothelial dysfunction beyond the heart. *Eur Heart J* 2018;**39**:4098–4100. https://doi.org/10.1093/eurheartj/ehy576
2. Chiu JJ, Chien S. Effects of disturbed flow on vascular endothelium: pathophysiological basis and clinical perspectives. *Physiol Rev* 2011;**91**:327–387. https://doi.org/10.1152/physrev.00047.2009
3. Kwak BR, Back M, Bochaton-Piallat ML, Caligiuri G, Daemen MJ, Davies PF, *et al.* Biomechanical factors in atherosclerosis: mechanisms and clinical implications. *Eur Heart J* 2014;**35**:3013–3020, 3020a–3020d. https://doi.org/10.1093/eurheartj/ehu353
4. Zhou J, Lee PL, Tsai CS, Lee CI, Yang TL, Chuang HS, *et al.* Force-specific activation of Smad1/5 regulates vascular endothelial cell cycle progression in response to disturbed flow. *Proc Natl Acad Sci USA* 2012;**109**:7770–7775. https://doi.org/10.1073/pnas.1205476109
5. Boo YC, Sorescu G, Boyd N, Shiojima I, Walsh K, Du J, *et al.* Shear stress stimulates phosphorylation of endothelial nitric-oxide synthase at Ser1179 by Akt-independent mechanisms: role of protein kinase A. *J Biol Chem* 2002;**277**:3388–3396. https://doi.org/10.1074/jbc.M108789200
6. Hambrecht R, Adams V, Erbs S, Linke A, Krankel N, Shu Y, *et al.* Regular physical activity improves endothelial function in patients with coronary artery disease by increasing phosphorylation of endothelial nitric oxide synthase. *Circulation* 2003;**107**:3152–3158. https://doi.org/10.1161/01.CIR.0000074229.93804.5C
7. Grashoff C, Hoffman BD, Brenner MD, Zhou R, Parsons M, Yang MT, *et al.* Measuring mechanical tension across vinculin reveals regulation of focal adhesion dynamics. *Nature* 2010;**466**:263–266. https://doi.org/10.1038/nature09198
8. Parsons JT, Horwitz AR, Schwartz MA. Cell adhesion: integrating cytoskeletal dynamics and cellular tension. *Nat Rev Mol Cell Biol* 2010;**11**:633–643. https://doi.org/10.1038/nrm2957
9. Carisey A, Ballestrem C. Vinculin, an adapter protein in control of cell adhesion signalling. *Eur J Cell Biol* 2011;**90**:157–163. https://doi.org/10.1016/j.ejcb.2010.06.007
10. Kaushik G, Spenlehauer A, Sessions AO, Trujillo AS, Fuhrmann A, Fu Z, *et al.* Vinculin network-mediated cytoskeletal remodeling regulates contractile function in the aging heart. *Sci Transl Med* 2015;**7**:292ra299. https://doi.org/10.1126/scitranslmed.aaa5843
11. Bays JL, DeMali KA. Vinculin in cell-cell and cell-matrix adhesions. *Cell Mol Life Sci* 2017;**74**:2999–3009. https://doi.org/10.1007/s00018-017-2511-3
12. Kristensen LP, Larsen MR, Mickley H, Saaby L, Diederichsen AC, Lambrechtsen J, *et al.* Plasma proteome profiling of atherosclerotic disease manifestations reveals elevated levels of the cytoskeletal protein vinculin. *J Proteomics* 2014;**101**:141–153. https://doi.org/10.1016/j.jprot.2013.12.011
13. Mayor F, Cruces-Sande M, Arcones AC, Vila-Bedmar R, Briones AM, Salaices M, *et al.* G protein-coupled receptor kinase 2 (GRK2) as an integrative signalling node in the regulation of cardiovascular function and metabolic homeostasis. *Cell Signal* 2018;**41**:25–32. https://doi.org/10.1016/j.cellsig.2017.04.002
14. Malhotra R, D'Souza KM, Staron ML, Birukov KG, Bodi I, Akhter SA. G alpha(q)-mediated activation of GRK2 by mechanical stretch in cardiac myocytes: the role of protein kinase C. *J Biol Chem* 2010;**285**:13748–13760. https://doi.org/10.1074/jbc.M110.109272
15. Huveneers S, Oldenburg J, Spanjaard E, van der Krogt G, Grigoriev I, Akhmanova A, *et al.* Vinculin associates with endothelial VE-cadherin junctions to control force-dependent remodeling. *J Cell Biol* 2012;**196**:641–652. https://doi.org/10.1083/jcb.201108120
16. Stary HC, Chandler AB, Dinsmore RE, Fuster V, Glagov S, Insull W Jr, *et al.* A definition of advanced types of atherosclerotic lesions and a histological classification of atherosclerosis. A report from the Committee on Vascular Lesions of the Council on Arteriosclerosis, American Heart Association. *Circulation* 1995;**92**:1355–1374. https://doi.org/10.1161/01.cir.92.5.1355
17. Bart BA, Shaw LK, McCants CBJR, Fortin DF, Lee KL, Califf RM, *et al.* Clinical determinants of mortality in patients with angiographically diagnosed ischemic or nonischemic cardiomyopathy. *J Am Coll Cardiol* 1997;**30**:1002–1008. https://doi.org/10.1016/s0735-1097(97)00235-0
18. Murga C, Arcones AC, Cruces-Sande M, Briones AM, Salaices M, Mayor F Jr. G protein-coupled receptor kinase 2 (GRK2) as a potential therapeutic target in cardiovascular and metabolic diseases. *Front Pharmacol* 2019;**10**:112. https://doi.org/10.3389/fphar.2019.00112
19. Wei SY, Shih YT, Wu HY, Wang WL, Lee PL, Lee CI, *et al.* Endothelial yin yang 1 phosphorylation at S118 induces atherosclerosis under flow. *Circ Res* 2021;**129**:1158–1174. https://doi.org/10.1161/CIRCRESAHA.121.319296
20. Demos C, Williams D, Jo H. Disturbed flow induces atherosclerosis by annexin A2-mediated integrin activation. *Circ Res* 2020;**127**:1091–1093. https://doi.org/10.1161/CIRCRESAHA.120.317909
21. Sorokin V, Vickneson K, Kofidis T, Woo CC, Lin XY, Foo R, *et al.* Role of vascular smooth muscle cell plasticity and interactions in vessel wall inflammation. *Front Immunol* 2020;**11**:599415. https://doi.org/10.3389/fimmu.2020.599415
22. Li Y, Zhu H, Zhang Q, Han X, Zhang Z, Shen L, *et al.* Smooth muscle-derived macrophage-like cells contribute to multiple cell lineages in the atherosclerotic plaque. *Cell Discov* 2021;**7**:111. https://doi.org/10.1038/s41421-021-00328-4
23. Kawakami K, Fujita Y, Kato T, Mizutani K, Kameyama K, Tsumoto H, *et al.* Integrin beta4 and vinculin contained in exosomes are potential markers for progression of prostate cancer associated with taxane-resistance. *Int J Oncol* 2015;**47**:384–390. https://doi.org/10.3892/ijo.2015.3011
24. Serrano K, Devine DV. Vinculin is proteolyzed by calpain during platelet aggregation: 95 kDa cleavage fragment associates with the platelet cytoskeleton. *Cell Motil Cytoskeleton* 2004;**58**:242–252. https://doi.org/10.1002/cm.20011
25. Nilsson J. Atherosclerotic plaque vulnerability in the statin era. *Eur Heart J* 2017;**38**:1638–1644. https://doi.org/10.1093/eurheartj/ehx143
26. Payne S, De Val S, Neal A. Endothelial-specific Cre mouse models. *Arterioscler Thromb Vasc Biol* 2018;**38**:2550–2561. https://doi.org/10.1161/ATVBAHA.118.309669
27. Gallino A, Aboyans V, Diehm C, Cosentino F, Stricker H, Falk E, *et al.* Non-coronary atherosclerosis. *Eur Heart J* 2014;**35**:1112–1119. https://doi.org/10.1093/eurheartj/ehu071